

Total-Reaction-Cross-Section Measurements for 30–60-MeV Protons and the Imaginary Optical Potential*

J. J. H. Menet,† E. E. Gross, J. J. Malanify,‡ and A. Zucker§

Oak Ridge National Laboratory, Oak Ridge, Tennessee 37830

(Received 7 May 1971)

We have measured total reaction cross sections for 30-, 40-, 49.5-, and 60.8-MeV protons incident on thin, separated isotopes covering the range from ^{12}C to ^{208}Pb . Our results are consistent with previous data at 30 MeV, but disagree with earlier data at 60 MeV. We find a strong dependence of the reaction cross section on neutron excess for a series of Fe and Ni isotopes. Little, if any, such dependence is observed for the $N=28$ isotones. The data are well represented by the relation $\sigma_R = \pi(r_0 A^{1/3} + \bar{\lambda})^2$ with $r_0 = 1.23 \pm 0.01$ F. When analyzed with the conventional optical model, our data require the volume absorption to increase and the surface absorption to decrease with increasing proton energy E_p . The analysis reveals a striking $(N-Z)/A$ dependence for the product $W_D a'$. Using the Oak Ridge parameters for the real and spin-orbit potentials, we arrive at the following parametrization for the imaginary potential: volume absorption potential, $W_0 = (1.2 + 0.09 E_p)$ MeV; surface absorption potential, $W_D = [4.2 - 0.05 E_p + 15.5 (N-Z)/A]$ MeV; imaginary diffusivity, $a' = [0.74 - 0.008 E_p + 1.0 \times (N-Z)/A]$ F.

I. INTRODUCTION

During the past few years systematic studies of proton elastic scattering and polarization between 30 and 60 MeV have provided a great deal of new information about the nuclear optical model. Surveys of data between 30 and 60 MeV¹⁻³ have successfully constructed optical models with very similar parameters, wherein the geometry was held fixed and only the strengths of the potentials were allowed to vary as a function of energy E_p , atomic number A , and neutron excess $\epsilon = (N-Z)/A$. The systematics of the real and spin-orbit potentials seemed very encouraging, but because the data used in these studies included only scattering and polarization, the imaginary part of the potential could not be pinned down to any reasonably systematic behavior. True, scattering and polarization results do affect the imaginary potential, but it was readily apparent that accurate values of the total reaction cross section σ_R were needed to achieve greater sensitivity in the imaginary potential. To obtain more data relevant to the choice of imaginary parameters was the principal motivation for our measurements. There were, however, two additional reasons for embarking on this piece of research.

When we examined the entire corpus of total-reaction-cross-section measurements for protons, a startling fact became apparent when the cross sections were plotted as a function of energy, Fig. 1. Measurements⁴⁻¹² between 10 and 30 MeV agree reasonably well with predictions of an optical model, even though the accuracy in many cases was not sufficient to determine the imaginary parameters definitively. Above 30 MeV, and specifically

at 60 MeV, the measured¹³ cross sections were inconsistent with an optical potential that fits¹ elastic scattering and polarization data at 30 and 40 MeV and elastic scattering data at 61.4 MeV.¹⁴ Furthermore the 60-MeV proton results were about 30% lower than total reaction cross sections measured¹⁵ with 55-MeV neutrons. We concluded that either the measurements of σ_R for 60-MeV protons were grossly in error, or that the optical model was breaking down in this region. Each of these possibilities justified a reexamination of the energy region between 30 and 60 MeV with new techniques.

Finally, recent measurements by Dicello, Igo, and Roush¹¹ at 14.5 MeV showed that σ_R was strongly dependent on the number of neutrons in the Fe, Ni, and Zn isotopes. In fact it was noticed by several authors^{3,16,17} that satisfactory fits to the reaction cross section could be obtained by including an $(N-Z)/A$ dependence in the imaginary diffuseness term of the potential. For this reason we concluded that it would be interesting to look at the dependence of σ_R on the neutron excess at energies above 30 MeV.

We report in this paper measurements of the proton total reaction cross section for several nuclei from ^{12}C to ^{208}Pb at $E_p = 30.0, 40.0, 49.5,$ and 60.8 MeV with three goals in mind: (1) to get a better understanding of the imaginary part of the potential, (2) to look for the sharp dip in σ_R between 30 and 60 MeV, and (3) to investigate the dependence of σ_R with the neutron excess in isotopic chains. Initial measurements at 60.8 MeV have been previously reported¹⁸ and confirmed our suspicion regarding the earlier experiment.¹³ An improvement in the measurement reported herein supplants the previous results at 60.8 MeV.

II. EXPERIMENTAL

A. General Method

The classical method to measure proton total reaction cross sections in this energy range is the anticoincidence beam-attenuation technique introduced by Gooding.⁴ The number of protons incident on the target is measured by a set of counters that we will call 1, and those that have not interacted with the target are detected by a stopping counter 2, which subtends a large solid angle (see Fig. 2). If the nuclear reactions made by the protons in counter 2 are neglected, then the anticoincidence of 2 with 1 is proportional to the total reaction cross section: $\sigma_R \propto (1\bar{2})$. The labels 1 and 2 indicate the number of protons detected by counters 1 and 2, respectively. A bar above a number implies that that counter is in anticoincidence. However, the number of nuclear reactions due to the protons absorbed in counter 2 cannot be neglected; in fact, they are the origin of most of the events $1\bar{2}$. As an example, at 60 MeV, using a 20 mg/cm² target of ¹²⁰Sn, $(1\bar{2})/1 = 5 \times 10^{-2} + 10^{-4}$, where 5×10^{-2} is due to the nuclear reactions in counter 2 and 10^{-4} is the fraction of protons removed from the beam by the target. To account for the reactions in counter 2, the measurement is repeated with the target removed and

$$\sigma_R \propto [(1\bar{2})/1]_{\text{target in}} - [(1\bar{2})/1]_{\text{target out}}.$$

Due to the large number of reactions in 2, relative to the number of reactions in the target, many

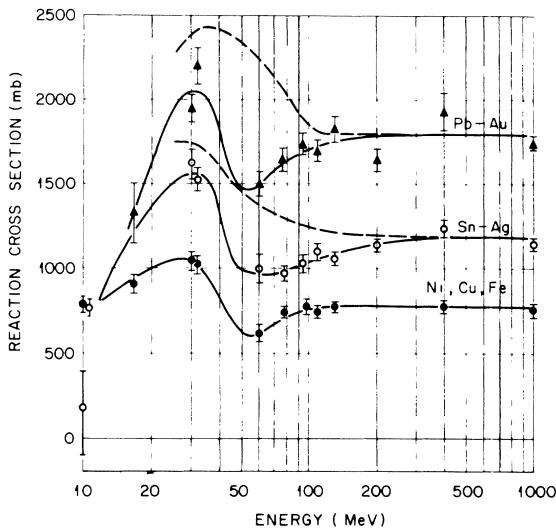


FIG. 1. Variation of proton total reaction cross section with proton energy for three mass regions. The solid curves indicate the trend of the data before the present experiment. The dashed curve indicates the trend of neutron total-reaction-cross-section measurements with energy.

protons must be counted to obtain a desired statistical accuracy. In our example, above, to achieve an accuracy of 4%, 3×10^8 protons are needed in both target-in and target-out measurements. The stopping detector, however, can accept only about 5×10^3 protons/sec, because above this rate the gain of the photomultiplier shifts with counting rate. With this counting rate a single reaction cross-section determination requires about 300 h of running time.

To reduce the counting time, earlier studies have often resorted to target thicknesses corresponding to 3- to 10-MeV energy loss for protons between 30 and 60 MeV. This, however, leads to another difficulty, since the proton energy at counter 2 is different for the target-in measurement than for the target-out measurement. As the number of reactions in counter 2 is energy-dependent, a simple target-out measurement does not give the correct number due to reactions in 2. To eliminate this effect an absorber is usually placed in front of the apparatus when the target-out measurement is made. The energy loss in the absorber is chosen such that the energy of the proton is the same in counter 2 for a target-in and a target-out measurement. It must be emphasized that this leads to serious difficulties, because the proton energy is now different at counter 1 when the target is in and when the target is out. An event in counter 1 does not necessarily mean that the proton will hit the target, since some protons will scatter in counter 1 through an angle larger than is subtended by counter 2. This scattering is energy-dependent and therefore is not canceled by a target-in and target-out measurement. It is difficult to evaluate the magnitude of this scattering effect since it depends on the fabrication details of counter 1 and the details of beam preparation. However, errors as large as 30% can be introduced by this process. All these considerations explain why reaction cross sections are difficult to measure in this proton energy range.

In this experiment we use an improved method first reported by Dicello *et al.*,¹¹ which depends on

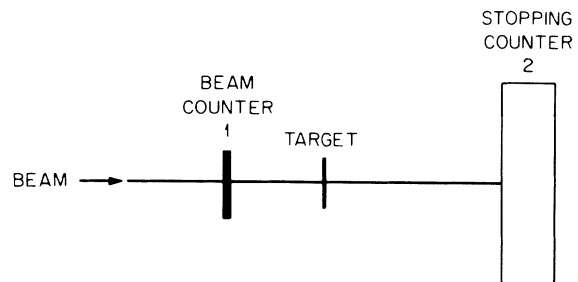


FIG. 2. Classic arrangement for measurement of total reaction cross sections by the beam-attenuation method.

the assumption that the number of charged reaction products at very forward angles can be neglected. The improvement made by Dicello, Igo, and Roush consists of replacing the stopping counter 2 in Fig. 2 by two counters – counters 4 and 5 of Fig. 3. The first counter is a thin ΔE detector subtending a small solid angle with respect to the target. In our case, the angle between the outer edge of counter 4 and the center of the target is 11° . The second counter, counter 5 in Fig. 3, is a stopping counter which detects protons scattered in the angular range $11^\circ < \theta < 45^\circ$. In this arrangement most of the protons are detected by a thin rather than a thick counter. Protons which have passed through counter 4 are prevented from reaching counter 5 by a nickel absorber. This scheme has two advantages: first is a reduction in the number of nuclear reactions in the detector. For a 2-MeV-thick counter, 10^{-3} of the incoming protons make nuclear reactions which are not detected; this is to be compared with the number 5×10^{-2} above. The second advantage is that the counting rate in counter 4 can be increased, since the protons now lose only a small part of their energy. These improvements allowed us to measure reaction cross sections to 4% accuracy in about 30 min, and to use 200-keV-thick targets instead of the 3- to 10-MeV thicknesses used before.

Our experimental apparatus is shown schematically in Fig. 3. Three counters labeled 1, 2, and 3 define the number of incoming protons; all the counters are NE102 plastic scintillators connected to Amperex XP1110 photomultipliers. Counters 1 and 2 are 0.38 mm thick, 5 mm in diameter. Counter 3 is 2 mm thick and has a hole 5 mm in diameter in the middle; most of the protons go through the hole and are not detected by counter 3. Counter 3 subtends an angle of $\pm 30^\circ$ measured from coun-

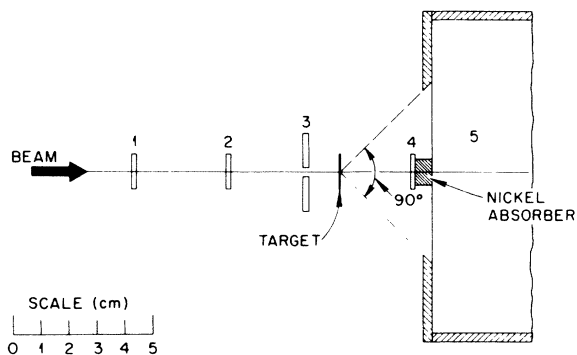


FIG. 3. Improved method (Ref. 11) for measuring proton total reaction cross sections. Only the distances between counters are to scale as used in the present experiment.

ter 2. The event $12\bar{3}$ defines a proton incident on the target. A proton detected in counters 1 and 2, but scattered from the latter through more than 30° , is not detected by counter 3. Such an event might be considered a proton reacting in the target, but this event is canceled by a target-in and target-out run, provided the energy of the beam is the same in both cases.

B. Electronics

A schematic diagram of the electronics is shown in Fig. 4. The rise time of the linear signal from the five counters is typically 3 nsec. The energy resolution of counters 1 and 2 is about 10% and the discriminator levels are set close to the proton peak. Because of the geometry of counter 3 the energy resolution of its spectrum is poor, and in order to detect the maximum number of protons in 3, the discriminator level is set as close as possible to the noise of the photomultiplier. The logic pulses from counters 1, 2, and 3 feed a coincidence circuit; the width of the coincidence pulse is typically 8 nsec; the width of the anticoincidence pulse is about 25 nsec. The dead time of the discriminator can be neglected. The signature $12\bar{3}$ defines the number of protons incident on the target. This signal goes to a fast scaler as well as to a coincidence circuit, whose other input is $\bar{4}$. The coincidence pulse corresponding to $12\bar{3}\bar{4}$ goes to a scaler and is also used to make a coincidence with a pulse from counter 5. The linear pulses from counter 5 which are in coincidence with the logic signal $12\bar{3}\bar{4}5$ go through the linear gate and are stored in a multichannel analyzer.

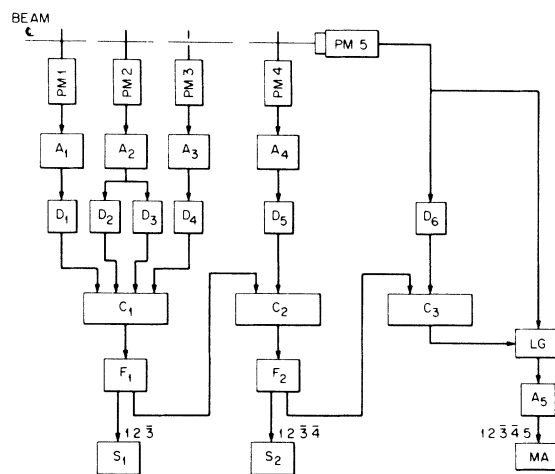


FIG. 4. Block diagram of the electronics: PM, photo tube; A, amplifier; D, discriminator; C, coincidence; F, fanout; LG, linear gate; S, scaler; MA, multichannel analyzer.

It is easily shown that

$$\sigma_M = \sigma_R + \sigma_{\text{elas}}^{\theta > 45^\circ} - \sigma_{\text{inelas}}^{\theta < 45^\circ} - \sigma_{\text{ch}}^{\theta < 11^\circ}$$

$$= \frac{1}{n} \frac{(12\bar{3}\bar{4})_{\text{in}} - (12\bar{3}\bar{4})_{\text{out}} - [(12\bar{3}\bar{4}\bar{5})_{\text{in}} - (12\bar{3}\bar{4}\bar{5})_{\text{out}}](1+k)}{(12\bar{3})}, \quad (1)$$

where:

σ_M is the experimentally observed cross section;

σ_R is the desired total reaction cross section;

$\sigma_{\text{elas}}^{\theta > 45^\circ}$ corresponds to the protons which were scattered elastically by the target through more than 45° ;

$\sigma_{\text{inelas}}^{\theta < 45^\circ}$ corresponds to the protons which were scattered inelastically on the target and are detected in counters 4 or 5;

$\sigma_{\text{ch}}^{\theta < 11^\circ}$ corresponds to all charged reaction products from the target inside an 11° cone;

n is the number of atoms per cm^2 in the target;

the labels "in" and "out" mean that the runs have been made with the target in the beam and removed from the beam;

k is the percentage of protons which undergo a nuclear reaction in 5 and are not identified as protons.

The runs "in" and "out" are made for the same number of incident protons.

Some low-energy contaminants in the beam can go through counter 1 and be stopped in counter 2. All these constitute spurious events $12\bar{3}$. This effect is canceled by target-in and target-out measurements.

We consider now the effect on the number of reactions in counter 4 due to the energy difference between target-in and target-out configurations. At 60 MeV, 5×10^{-3} protons incident on counter 4 make a nuclear reaction. Most of the charged particles resulting from proton reactions in counter 4 are, however, detected by this counter and the contribution of such an effect leads to $(12\bar{3}\bar{4})/(12\bar{3}) \approx 10^{-3}$ when the target is out. This ratio is energy-dependent. Therefore the energy of the beam has to be decreased by about 200 keV when the target is removed for the protons to have the same energy on counter 4. We have measured the effect $\rho = [(12\bar{3}\bar{4})/(12\bar{3})]_{\text{out}}$ at the energies E_p and $E_p - 200$ keV. For $E_p = 30, 40,$ and 60.8 MeV no change in ρ has been noticed within our statistical accuracy; we conclude that if there were an effect due to the two different energies on counter 4 when the target is in and out, this did not affect the reaction cross section by more than 1%. We estimate that for a

beam with an energy lowered by 200 keV for a target-out measurement, the effect on the ratio $[(12\bar{3})_{\text{in}} - (12\bar{3})_{\text{out}}]/(12\bar{3})$ is much smaller than 1% of the measured reaction cross sections.

In our experiment a discriminator is used on counter 4. The bias is set as low as possible in order to detect the maximum number of events due to nuclear reactions in counter 4. This reduced the ratio $(12\bar{3}\bar{4})/(12\bar{3})$ when the target is out and therefore increases the statistical accuracy of our measurement. For the same reason a single-channel analyzer is set on counter 2. We then eliminate a number of low-energy contaminants from the beam detected in counter 2, and reduce the ratio $(12\bar{3}\bar{4})/(12\bar{3})$ by a factor of 1.7 at 60 MeV. Another function of the single-channel analyzer on counter 2 is to eliminate events caused by two protons in a single beam burst.

Nuclear reactions also occur in counter 5. Protons are stopped in this counter at 60 MeV; 5×10^{-2} suffer nuclear reactions and are removed from the elastic peak. Fortunately only a very small fraction of the protons scattered by the target are detected in counter 5, and although the percentage of nuclear reactions in counter 5 is only known to 10%,¹⁹ this uncertainty affects the reaction-cross-section measurement by no more than 0.5% in the worst case.

We next consider random events. At 60.8 MeV the proton bursts are separated by 40 nsec, and their width is 1.5 nsec. If the resolving time plus the dead time of the electronics does not exceed 40 nsec, no random coincidences can occur. At lower energies, the bursts are separated by more than 40 nsec. This illustrates the advantage of such a high-duty-factor pulsed beam over both a low-duty-factor (e.g., proton linac) or dc (e.g., Van de Graaff) beam.

The assumption that the number of charged reaction products incident on counter 4 can be neglected depends on the accuracy desired for the measured cross section, on the yield of charged particles in the forward direction, and upon the solid angle subtended by counter 4. For a solid angle of ≈ 0.1 sr, this correction is certainly less than 1% at the energies used by Dicello, Igo, and Roush,¹¹ but at 60.8 MeV an extrapolation of data from Bertrand and Peelle²⁰ indicate that this correction could be as much as 5–10%. We have therefore measured the correction factor $\sigma_{\text{ch}}^{\theta < 11^\circ}$ for all tar-

gets at 40 and 60.8 MeV. This correction does not appear in our initial results at 60.8 MeV¹⁸ and the results presented here thus supercede the previous ones.

To evaluate this correction, we set a discriminator level on counter 4 so that we count only charged reaction products, including protons between 6 and 40 MeV for the 60.8-MeV measurements and protons between 6 and 28 MeV for the 40-MeV measurements. The inelastic protons missed because of this bias setting were estimated from the work of Bertrand and Peelle²⁰ to be less than 1% of the total reaction cross section. As before, an upper level discriminator on counter 2 eliminated events containing two protons in a single beam burst. The correction factor $\sigma_{ch}^{\theta < 11^\circ}$ is then given by

$$\sigma_{ch}^{\theta < 11^\circ} = \frac{1}{n} \frac{(12\bar{3}4)_{in} - (1234)_{out}}{12\bar{3}}$$

This correction is assumed to be negligible at 30 MeV and we interpolate the 40- and 60.8-MeV measurements to obtain this correction at 49.5 MeV.

C. Beam Setup

One of the most important procedures in this experiment is the preparation of the beam. The requirements are the following: The proton beam must have a very low intensity (10^5 protons/sec), and be relatively free of low-energy protons and

TABLE I. R is the ratio of the previously reported target thicknesses [Table I, Phys. Rev. **156**, 1207 (1967)] to the present thickness determination. The cross sections reported previously should be increased by these ratios.

Target	R
¹² C	1.036
⁵⁴ Fe	1.059
⁵⁸ Ni	1.148
⁵⁹ Co	1.104
⁶⁰ Ni	1.077
⁶⁸ Zn	1.200
⁹⁰ Zr	1.014
¹²⁰ Sn	1.153
²⁰⁸ Pb	1.032

all other charged particles. It must be stable in intensity and in position, and the size of the spot must not exceed 1 mm in diameter.

Figure 5 shows the schematic layout of the beam. The slits 1 and 2 had 2 mm × 2 mm openings and defined the angular divergence of the beam entering the 153° analyzing magnet. Their purpose was to reduce the beam intensity and to keep the spot from moving on the target. The 153° analyzing magnet defined the energy of the beam and removed most of the low-energy contaminants due to

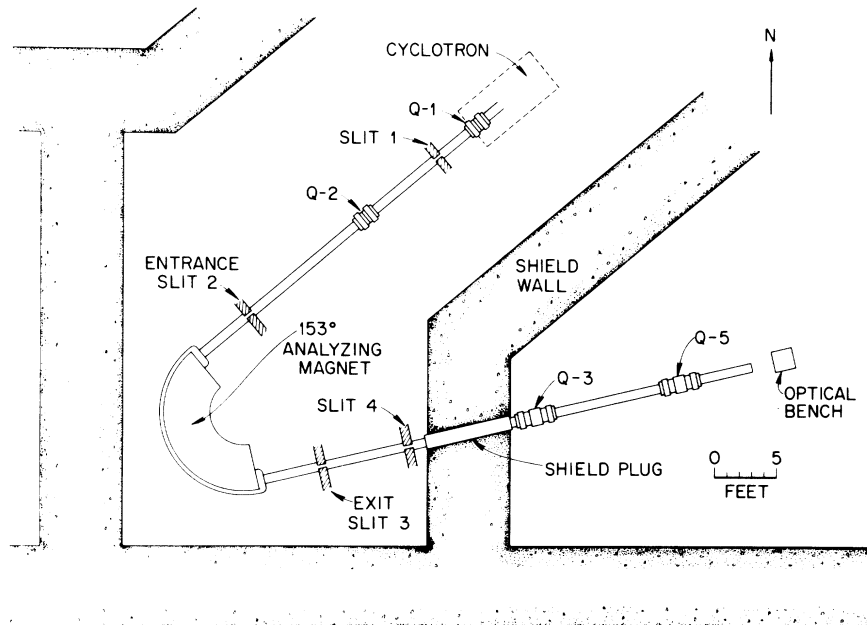


FIG. 5. Schematic layout of the beam optics.

slits 1 and 2. Slit 3 had a 2 mm \times 2 mm opening. The quadrupole lenses Q3 and Q5 transported the beam to the target, where we obtained a spot smaller than 1 mm diameter. The halo due to scattering on slit 3 was removed by slit 4. This slit scattering was further reduced by an intermediate focus between Q3 and Q5.

D. Targets

All the targets were isotopically enriched to at least 90%. Their thicknesses ranged between 3 and 26 mg/cm², with the exception of ¹²C which was 46.7 mg/cm² thick. An accurate measurement of the target thickness was made by measuring the energy loss, with a magnetic spectrometer, of a 20-MeV ³He beam passing through the target. An effort was made to measure the thickness for the same spot on the target that was used in the reaction-cross-section determination. The relative error is 2% for the thick targets and 5% for the thin ones.

The targets of ¹²C, ⁵⁴Fe, ⁵⁸Ni, ⁵⁹Co, ⁶⁰Ni, ⁶⁸Zn, ⁹⁰Zr, ¹²⁰Sn, and ²⁰⁸Pb were identical to those used in a previous optical-model study¹ and the new target-thickness determinations therefore modify the older cross-section measurements¹ by the multiplicative factors shown in Table I.

E. Running Procedure

The most sensitive component in this experiment was counter 4. Any change in its gain would affect the ratio $(12\bar{3}\bar{4})/(12\bar{3})$ and therefore the measurement of σ_R . The signal-to-noise ratio in counter 4 was typically 10; the level of the discriminator was set close to the noise of the tube. The energy resolution of the detector was about 15%.

To determine the optimum beam intensity to be used in the experiment, we studied the dependence of $\rho = (12\bar{3}\bar{4})/(12\bar{3})$ as a function of counting rate for ¹²C, see Fig. 6. No change in ρ , within our statistical accuracy, was evident at rates lower than 2×10^5 protons/sec. Above this value ρ was no longer constant. To avoid any trouble from beam intensity fluctuations we made our measurements

TABLE II. 30.0-MeV proton total reaction cross sections. Tabulated quantities are defined in Eq. (1) and in the text.

Target	σ_M (mb)	$\sigma_{\text{elas}}^{\theta > 45^\circ}$ (mb)	$\sigma_{\text{inelas}}^{\theta < 45^\circ}$ (mb)	σ_R (mb)
¹² C	508 \pm 10	61 \pm 10	...	447 \pm 20
⁵⁸ Ni	1067 \pm 18	82 \pm 10	26 \pm 10	1011 \pm 30
⁹⁰ Zr	1337 \pm 30	90 \pm 20	2 \pm 2	1249 \pm 45
¹²⁰ Sn	1670 \pm 42	91 \pm 15	10 \pm 5	1589 \pm 50
²⁰⁸ Pb	2253 \pm 57	141 \pm 20	5 \pm 3	2117 \pm 90

between 5×10^4 and 8×10^4 protons/sec. At this level our runs lasted 15 to 20 min. The spectrum of counter 4 was stored in a multichannel analyzer, to check the peak position after every run. The gain shift in counter 4 never exceeded 2% over a 12-h period. Since the rate in counter 4 was too high to be acceptable for multichannel analysis, we passed these pulses through a gate which was randomly opened about 100 times/sec. During a sequence of runs we constantly checked the stability of our equipment by checking the quantity

$$\xi = \frac{(12\bar{3}\bar{4})_{\text{out}} - (12\bar{3}\bar{4}5)_{\text{out}}}{(12\bar{3})_{\text{out}}}$$

for each target. Within statistical accuracy, the value of ξ was always constant for a given target.

After every run a plot of the spectrum of counter 5 was made. Since we were only interested in the elastic protons having the energy of the incoming beam, all the protons above a certain level, fixed arbitrarily on the plot, were counted. The level was 6 MeV below the full-energy proton peak. The number of protons above a level set 6 MeV below the elastic peak was determined and corrected for the number of reactions¹⁹ in counter 5.

With the exception of ¹²C at 30 and 40 MeV, the resolution of counter 5 was not good enough to resolve the inelastically scattered protons from levels below 6-MeV excitation. This correction is referred to as $\sigma_{\text{inelas}}^{\theta < 45^\circ}$ in Eq. (1) and was determined from inelastic scattering measurements.²¹⁻²⁹ Inelastic data were usually obtained at energies different from the ones we require. However, since

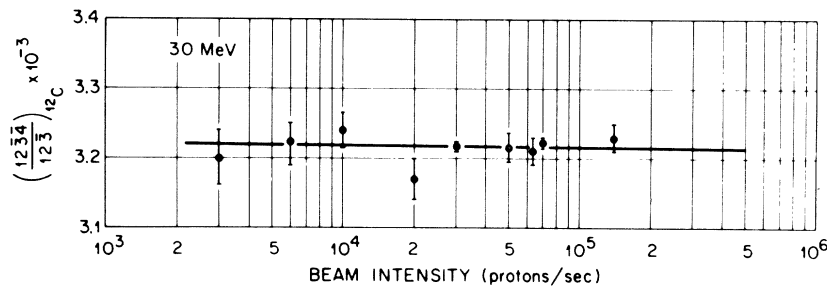


FIG. 6. The effect $\rho = (12\bar{3}\bar{4})/(12\bar{3})$ for ¹²C at 30 MeV as a function of beam intensity. For data accumulation we operated at beam intensities between 5 and 8×10^4 protons/sec.

TABLE III. 40.0-MeV proton total reaction cross sections. Tabulated quantities are defined in Eq. (1) and in the text.

Target	σ_M (mb)	$\sigma_{\text{elas}}^{\theta > 45^\circ}$ (mb)	$\sigma_{\text{inelas}}^{\theta < 45^\circ}$ (mb)	$\sigma_{\text{ch}}^{\theta < 11^\circ}$ (mb)	σ_R (mb)
^{12}C	395 ± 4	36 ± 5	...	12 ± 4	371 ± 11
^{27}Al	638 ± 25	66 ± 6	25 ± 10	48 ± 15	645 ± 35
^{58}Ni	922 ± 18	59 ± 5	26 ± 10	66 ± 20	955 ± 34
^{60}Ni	994 ± 30	54 ± 5	15 ± 7	27 ± 20	982 ± 42
^{62}Ni	1055 ± 70	54 ± 15	18 ± 10	55 ± 40	1074 ± 90
^{64}Ni	1087 ± 65	54 ± 15	11 ± 6	42 ± 40	1089 ± 90
^{54}Fe	860 ± 30	61 ± 10	6.5 ± 4	50 ± 20	856 ± 37
^{56}Fe	1014 ± 37	61 ± 10	11 ± 6	27 ± 20	991 ± 43
^{57}Fe	1015 ± 110	61 ± 10	...	170 ± 70	1124 ± 130
^{58}Fe	1265 ± 120	61 ± 10	18 ± 10	100 ± 50	1313 ± 130
^{59}Co	1038 ± 42	57 ± 6	5 ± 3	56 ± 30	1042 ± 52
^{68}Zn	1230 ± 45	45 ± 5	27 ± 10	18 ± 27	1230 ± 54
^{90}Zr	1380 ± 60	66 ± 6	2 ± 2	0 ± 25	1316 ± 65
^{120}Sn	1598 ± 60	68 ± 6	10 ± 5	78 ± 40	1618 ± 73
^{208}Pb	2078 ± 90	62 ± 6	5 ± 3	2 ± 40	2023 ± 100

TABLE IV. 49.5-MeV proton total reaction cross sections. Tabulated quantities are defined in Eq. (1) and in the text. $\sigma_{\text{ch}}^{\theta < 11^\circ}$ (mb) values are interpolated from the measurements at 40 and 60.8 MeV.

Target	σ_M (mb)	$\sigma_{\text{elas}}^{\theta > 45^\circ}$ (mb)	$\sigma_{\text{inelas}}^{\theta < 45^\circ}$ (mb)	$\sigma_{\text{ch}}^{\theta < 11^\circ}$ (mb)	σ_R (mb)
^{12}C	318 ± 6	16 ± 5	35 ± 10	8 ± 4	345 ± 13
^{58}Ni	798 ± 16	30 ± 10	26 ± 10	62 ± 20	856 ± 29
^{90}Zr	1197 ± 48	35 ± 15	2 ± 2	50 ± 30	1214 ± 59
^{120}Sn	1446 ± 58	40 ± 15	10 ± 5	39 ± 40	1455 ± 72
^{208}Pb	1874 ± 70	45 ± 15	5 ± 3	8 ± 60	1842 ± 93

TABLE V. 60.8-MeV proton total reaction cross sections. Tabulated quantities are defined in Eq. (1) and in the text.

Target	σ_M (mb)	$\sigma_{\text{elas}}^{\theta > 45^\circ}$ (mb)	$\sigma_{\text{inelas}}^{\theta < 45^\circ}$ (mb)	$\sigma_{\text{ch}}^{\theta < 11^\circ}$ (mb)	σ_R (mb)
^{12}C	266 ± 3	8 ± 2	35 ± 10	5 ± 3	310 ± 13
^{27}Al	479 ± 20	13 ± 2	25 ± 15	8 ± 10	499 ± 27
^{58}Ni	741 ± 17	17 ± 2	26 ± 10	57 ± 10	807 ± 25
^{60}Ni	798 ± 20	17 ± 10	15 ± 5	45 ± 15	841 ± 30
^{62}Ni	920 ± 49	17 ± 10	18 ± 10	56 ± 50	977 ± 76
^{64}Ni	1060 ± 45	17 ± 10	11 ± 6	9 ± 50	1063 ± 74
^{59}Co	789 ± 24	17 ± 10	5 ± 3	21 ± 15	798 ± 32
^{68}Zn	930 ± 27	17 ± 2	27 ± 10	8 ± 20	948 ± 38
^{54}Fe	733 ± 20	17 ± 10	6.5 ± 4	75 ± 20	798 ± 32
^{56}Fe	814 ± 20	17 ± 10	11 ± 6	91 ± 20	899 ± 32
^{57}Fe	744 ± 80	17 ± 10	...	56 ± 70	783 ± 120
^{58}Fe	908 ± 60	17 ± 10	18 ± 10	150 ± 57	1059 ± 90
^{50}Ti	774 ± 60	17 ± 10	20 ± 10	76 ± 60	853 ± 80
^{51}V	768 ± 26	17 ± 10	11 ± 6	25 ± 21	787 ± 35
^{52}Cr	707 ± 170	17 ± 10	18 ± 10	...	708 ± 190
^{90}Zr	1059 ± 26	23 ± 2	2 ± 2	106 ± 30	1144 ± 42
^{96}Zr	1264 ± 100	23 ± 10	1241 ± 150
^{116}Sn	1463 ± 40	20 ± 3	10 ± 5	0 ± 40	1453 ± 60
^{208}Pb	2004 ± 60	29 ± 3	5 ± 3	13 ± 60	1993 ± 95

these corrections were small, uncertainties in $\sigma_{\text{inelas}}^{\theta < 45^\circ}$ did not influence the reaction cross sections, cf. Tables II–V. The correction, taking into account those protons which were elastically scattered by the target through angles greater than 45° , is referred to as $\sigma_{\text{elas}}^{\theta > 45^\circ}$ in Eq. (1). This correction was deduced from the data reported in Refs. 1, 14, and the work of Ridley and Turner.³⁰ The 50-MeV values were interpolated from the 40- and 60-MeV results. Errors due to this procedure are not significant.

III. RESULTS

A. 30 MeV

In Table II we report the 30-MeV measurements for ^{12}C , ^{58}Ni , ^{90}Zr , ^{120}Sn , and ^{208}Pb . At this energy we have several points for comparison. Makino, Waddell, and Eisberg measured³¹ $\sigma_R = 396 \pm 19$ mb for ^{12}C at 28 MeV. They used a method analogous to that of Gooding.⁴ Cameron *et al.*³² found 430 ± 22 mb using the same technique as ours. For ^{58}Ni , our data are in accord with those of Refs. 31

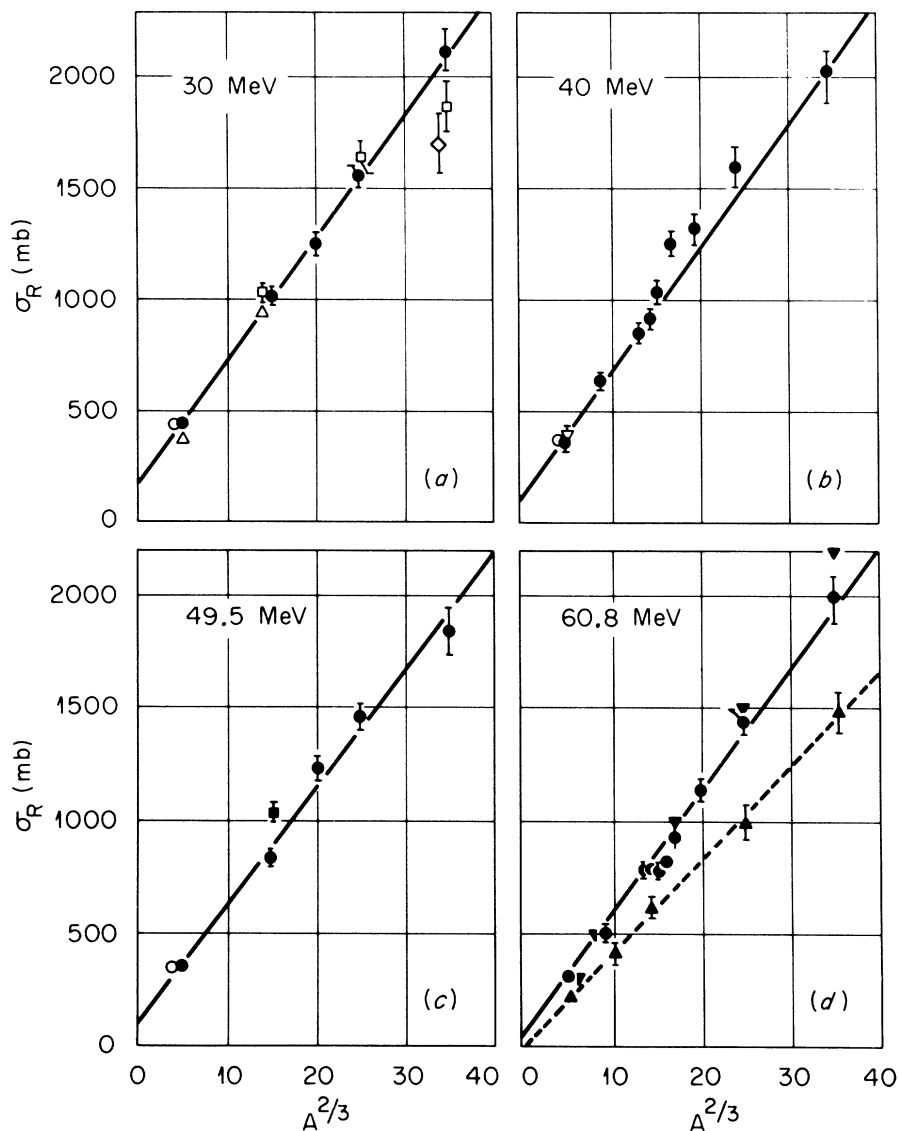


FIG. 7. (a)–(d) Proton total reaction cross sections at 30.0, 40.0, 49.5, and 60.8 MeV: ●, our data; ◇, Ref. 4; ■, Ref. 6; ▲, Ref. 13; ▼, Ref. 15; ○, Ref. 32; □, Ref. 33; △, Ref. 31; ▽, Ref. 34. The straight-line fits to our data are for the relation $\sigma_R = \pi(\tau_0 A^{1/3} + \bar{\lambda})^2$ where $\tau_0 = 1.23$ F.

and the work of Turner *et al.*³³ Their values are, respectively, $\sigma_R = 950 \pm 42$ mb and $\sigma_R = 1038 \pm 32$ mb. One measurement has been made on ^{120}Sn at 28.5 MeV³³; the value is $\sigma_R = 1638 \pm 68$ mb. In contrast, the same authors³³ find that for ^{208}Pb , $\sigma_R = 1865 \pm 98$ mb, a value incompatible with our result. One must note that our value for ^{208}Pb is close to that obtained for gold³¹ where $\sigma_R = 1983 \pm 121$ mb, as one might expect from neighboring nuclei.

In Fig. 7(a) we present our data as a function of $A^{2/3}$. The solid points correspond to our measurements, the open symbols to the results discussed above. It is evident that the results can be represented by a straight line. The low point for ^{208}Pb is due to a measurement of Gooding⁴ at 34 MeV.

B. 40 MeV

At this energy there are few points of comparison with our measurements. We are, however, in agreement with the measurement of Cameron *et al.*³² for ^{12}C , $\sigma_R = 386 \pm 19$ mb, as well as with Giles and Burge,³⁴ who find $\sigma_R = 405 \pm 38$ mb. Our results are again plotted as a function of $A^{2/3}$ in Fig. 7(b) and tabulated in Table III.

C. 49.5 MeV

The 49.5-MeV results are given in Table IV and displayed in Fig. 7(c). Two results can be compared with ours. The cross section for ^{12}C , if extrapolated from 24 and 46 MeV,³² yields a value $\sigma_R = 340 \pm 18$ mb. The cross section for ^{58}Ni was measured by Bearpark,⁶ who used a charge-collection method. We are completely at odds with his results, as he finds $\sigma_R = 1042 \pm 29$ mb. We ought to mention that our result for ^{58}Ni is consistent with the cross sections for other nuclei at this energy, since these are again represented by a straight line in Fig. 7. It is moreover surprising that Bearpark finds a larger value at 50 MeV than at 30 MeV, since one expects σ_R to decrease with increasing proton energy.

D. 60.8 MeV

Our results, tabulated in Table V, are compared with those of Meyer and collaborators¹³ in Fig. 7(d) (solid triangles). We are in complete disagreement with these authors. Our values of σ_R are systematically 20 to 30% higher than theirs. It appears that Meyer, Eisberg, and Carlson are the victims of a systematic error. They measured the cross section at 61-MeV incident energy on targets about 10 MeV thick. In the runs with the target out they introduce in front of their apparatus a 10-MeV-thick absorber. Under these conditions the number of reactions in the detector following the

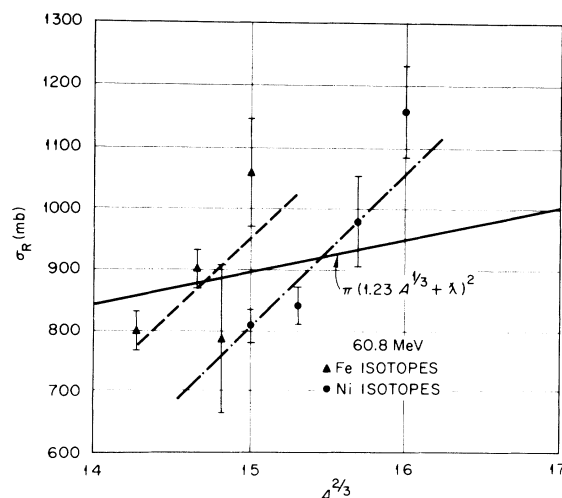


FIG. 8. Fe and Ni isotope data at 60.8 MeV plotted as a function of $A^{2/3}$. The solid line shows the trend of the data for a large mass range from Fig. 7(d), while the broken lines show the trends for the Fe and Ni isotopes.

target was the same whether the target was in or out. Unfortunately, the beam energy was different in the first ΔE detector, depending on whether the target was in or out; the number of protons scattered by that detector was therefore not the same in the two cases and the target-in and target-out measurements cannot eliminate this difference. From the geometry of their apparatus and the thickness of their ΔE counters, we have estimated

TABLE VI. Comparison of present (Oak Ridge) zero-parameter model with that of Becchetti and Greenlees, Ref. 3. χ^2/N values only include contributions from elastic scattering cross sections and polarization data, where available.

Target	E_p (MeV)	$\sigma_{R \text{ exp}}$ (mb)	χ^2/N	Oak Ridge $\sigma_{R \text{ calc}}$	Becchetti and Greenlees χ^2/N	$\sigma_{R \text{ calc}}$
^{58}Ni	30.0	1011 ± 30	40	1050	34	1087
^{120}Sn	30.0	1589 ± 50	38	1698	49	1629
^{208}Pb	30.0	2117 ± 90	22	2042	39	1907
^{54}Fe	40.0	856 ± 37	35	917	23	947
^{58}Ni	40.0	955 ± 34	44	950	58	982
^{58}Co	40.0	1042 ± 52	12.5	1049	13	1065
^{68}Zn	40.0	1230 ± 54	36	1192	32	1189
^{90}Zr	40.0	1316 ± 65	27	1350	25	1349
^{120}Sn	40.0	1618 ± 73	22.5	1658	18	1653
^{208}Pb	40.0	2023 ± 100	38	2131	94	2054
^{27}Al	61.4	499 ± 27	8.9	461	2.5	544
^{58}Ni	61.4	807 ± 25	12.1	788	2.9	893
^{68}Zn	61.4	948 ± 38	27.3	987	18.5	1028
^{90}Zr	61.4	1144 ± 42	11.9	1163	8.6	1211
^{116}Sn	61.4	1453 ± 60	12.3	1399	13.2	1433

the systematic error to which their experiment was subject, and we conclude that it would indeed reduce their cross sections by about 20%, a value which is not in disagreement with the difference between their results and ours. Our results appear compatible with reaction cross sections measured¹⁵ with 55-MeV neutrons and these measurements are also shown in Fig. 7(d).

IV. DISCUSSION OF RESULTS

In Fig. 7 our results are presented as a function of $A^{2/3}$. One can compare them with the expression

$$\sigma_R = \pi(r_0 A^{1/3} + \bar{\lambda})^2,$$

where $\bar{\lambda}$ corresponds to the de Broglie wave length of the incident proton. We note that the slope of the straight lines is the same for the four energies, and this slope leads to a value of $r_0 = 1.23 \pm 0.01$ F where the error is a standard deviation from the average value.

Our results are in reasonable agreement with the predictions of the optical-model analysis of Fulmer *et al.*,¹⁴ although their values for σ_R are slightly higher than the experimentally observed ones. In addition, we now find that there is no disagreement between total reaction cross sections of protons and neutrons near 60 MeV and also that there is no minimum in the curve when the reaction cross section is plotted as a function of energy (Fig. 1). In fact, σ_R decreases slowly between 30

and 60 MeV in about the same way as it does for neutrons.

In our measurements at 40 and 60.8 MeV we have studied in greater detail the isotopes of iron and nickel. The 60.8-MeV results are shown in Fig. 8, again plotted as a function of $A^{2/3}$. The solid straight line is the curve for all elements from carbon to lead. It is particularly interesting to find that for the isotopes of iron and nickel σ_R varies much more rapidly with A than the best fit to all the 60.8-MeV data. The same effect is apparent at 40 MeV. When we plot our results as a function of $\epsilon = (N - Z)/A$ (Figs. 9 and 10), the dependence on this parameter is startling and confirms the findings of Dicello, Igo, and Roush at 14.5 MeV.¹¹ These authors have found the same behavior of σ_R for the isotopes of iron, nickel, and zinc. Another interesting point which appears in Figs. 9 and 10 is that the dependence of the cross section on $(N - Z)/A$ is the same at 40 and 60.8 MeV as it is at 14.5 MeV.¹¹ At these three energies the differences between the extreme values of ϵ are, respectively, 265 ± 25 , 285 ± 40 , and 235 ± 40 mb. In contrast to this behavior, our measurements for the $N = 28$ isotones, Fig. 11, show little if any variation of the proton reaction cross section with A . The isotope and isotone behavior may be regarded either as evidence for a neutron-rich nuclear surface or simply as a consequence of the p - n interaction being several times stronger than the p - p interaction.³⁵ Although data and analysis concerning the nuclear surface continues to mount, there is as yet no conclusive evidence for either a neutron- or a proton-rich surface in nuclei.³⁶

It is interesting to examine the optical-model parameters which predict an $(N - Z)/A$ dependence

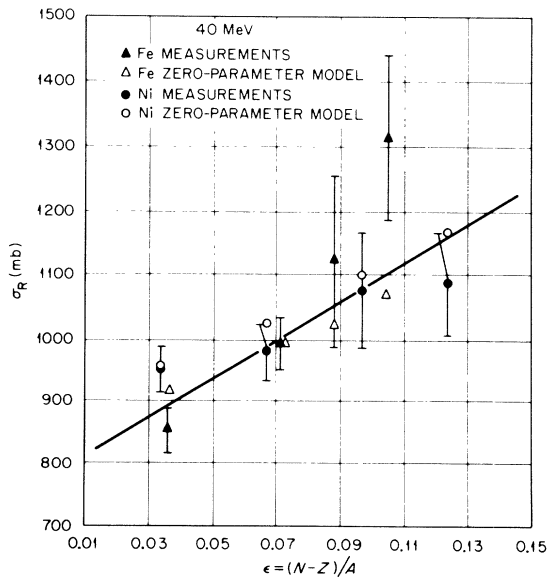


FIG. 9. Fe and Ni isotope data at 40 MeV vs $\epsilon = (N - Z)/A$. The solid line indicates the trend of the data. The open symbols are calculated from the zero-parameter model derived from an optical-model analysis of the new data.

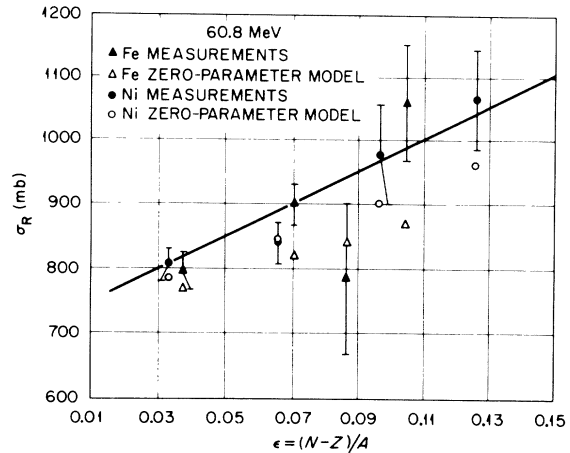


FIG. 10. Fe and Ni isotope data at 60.8 MeV versus $\epsilon = (N - Z)/A$. The solid line indicates the trend of the data. The open symbols are values calculated from our zero-parameter optical model.

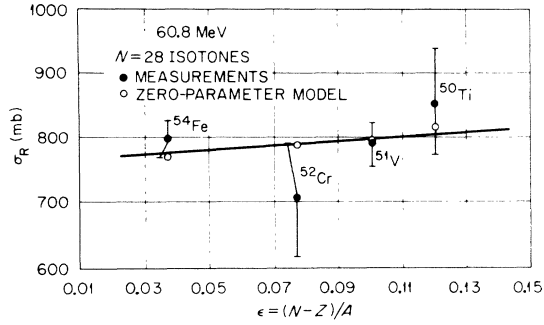


FIG. 11. 60.4-MeV proton total reaction cross sections for $N=28$ isotones plotted as a function of $\epsilon = (N-Z)/A$. The open circles are values calculated from our zero-parameter optical model.

for the reaction cross section. A detailed study by Perey³⁷ on elastic scattering of protons between 9 and 22 MeV shows that the real part of the potential should include a symmetry term which, however, does not suffice to explain the observed vari-

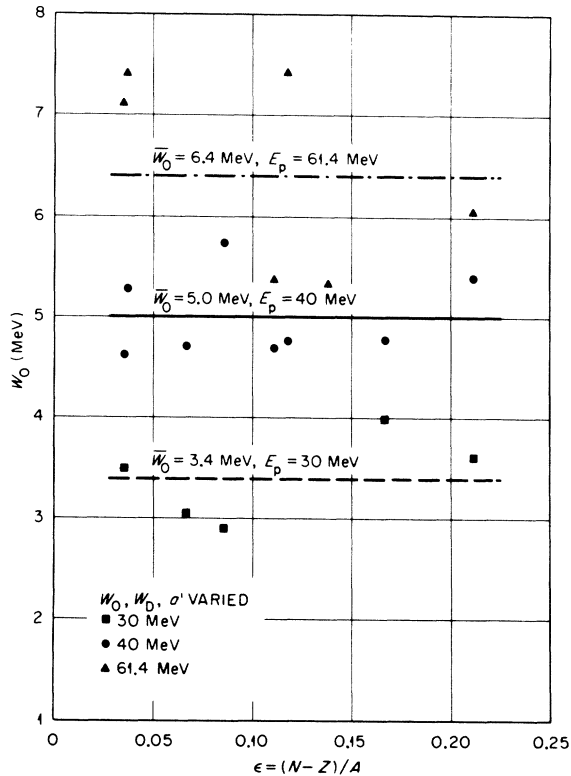


FIG. 12. Values of the volume absorption potential, W_0 , from a three-parameter (W_0 , W_D , and a') optical-model fit to 30-, 40-, and 61.4-MeV proton elastic scattering, polarization, and total-reaction-cross-section data. The remaining optical-model parameters were taken from Ref. 1. Also shown are average values of W_0 at the three energies.

ation of σ_R with $(N-Z)/A$. Because σ_R is particularly sensitive^{16, 17} to the imaginary diffuseness a' , it is tempting to include the symmetry parameter $(N-Z)/A$ in the expression for a' . This was done, for example, in a recent analysis by Becchetti and Greenlees³ and was suggested also by Satchler.³⁸ Since the number of absorptions on the nuclear surface is proportional to the product $W_D a'$, an $(N-Z)/A$ dependence can be ascribed to W_D ^{3, 17} instead of, or in addition to, such a dependence for a' . In the optical-model analysis to follow, we pursue these points further using our reaction-cross-section data as a sensitive probe of the imaginary optical-model parameters.

V. OPTICAL-MODEL ANALYSIS

One of our objectives in measuring a large number of reaction cross sections was to provide suitable data for establishing trends in the imaginary part of the optical potential. In particular, we look for trends in the imaginary volume potential W_0 , the imaginary surface potential W_D , and the imagi-

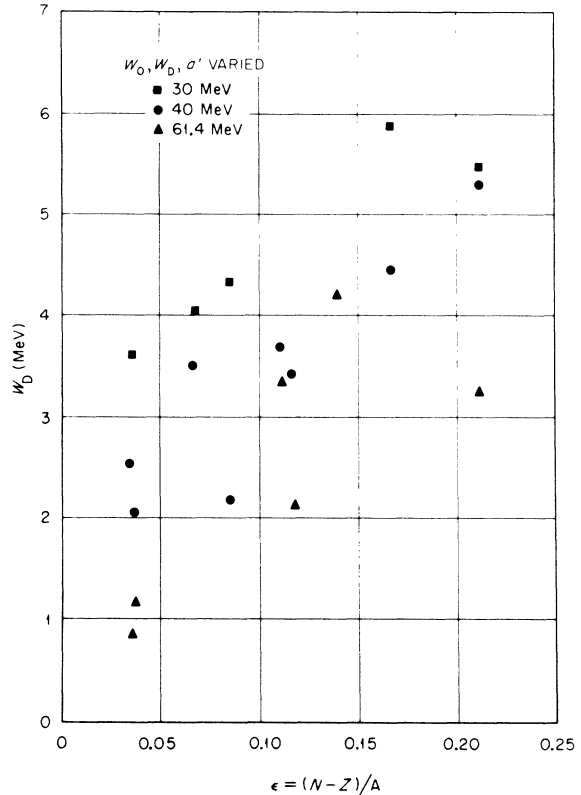


FIG. 13. Values of the surface absorption potential, W_D , versus $\epsilon = (N-Z)/A$ from a three-parameter (W_0 , W_D , and a') optical-model fit to 30-, 40-, and 61.4-MeV proton elastic scattering, polarization, and total-reaction-cross-section data. The remaining optical-model parameters were taken from Ref. 1.

nary diffusivity a' . We thus take the view that the other optical-model parameters are rather well established in the 30–60-MeV range, since several analyses¹⁻³ give essentially the same parameters for these parts of the potential.

For the optical potential we use the standard form:

$$V(r) = V_C(r) + V_0 \frac{1}{e^{x^2} + 1} - i \left(W_0 - 4W_D \frac{d}{dx'} \right) \frac{1}{e^{x^2} + 1} + \left(\frac{\hbar}{m_\pi c} \right)^2 V_s \frac{1}{r} \frac{d}{dr} \frac{1}{e^{x_s^2} + 1} \vec{s} \cdot \vec{l}. \quad (2)$$

In Eq. (2) $V_C(r)$ is the Coulomb potential for a uniformly charged sphere of radius $1.25 A^{1/3}$ F, V_0 is the real potential, W_0 and W_D are the volume and surface parts, respectively, of the imaginary potential, and V_s is the real part of the spin-orbit potential. The imaginary part of the spin-orbit potential was always set to zero, since its value turns out to be very small in all cases we have encountered. The remaining factors in the optical potential contain the Woods-Saxon radius and diffusivity

parameters:

$$x = (r - R)/a, \quad R = r_0 A^{1/3},$$

$$x' = (r - R')/a, \quad R' = r'_0 A^{1/3},$$

$$x_s = (r - R_s)/a_s, \quad R_s = r_s A^{1/3},$$

and m_π is the pion rest mass.

We use the following Oak Ridge parameter set¹ which fits data reasonably well in the range 30–60 MeV:

$$\begin{aligned} r_0 &= 1.16 \text{ F}, & V_s &= 6.04 \text{ MeV}, \\ a &= 0.75 \text{ F}, & r_s &= 1.064 \text{ F}, \\ r'_0 &= 1.37 \text{ F}, & a_s &= 0.78 \text{ F}, \\ V_0 &= (49.9 - 0.22E_p + 0.4Z/A^{1/3} + 26.4\epsilon) \text{ MeV}, \end{aligned} \quad (3)$$

where E_p is the proton energy in MeV and $\epsilon = (N - Z)/A$ is the nuclear-symmetry parameter. We searched on these parameters again using the new cross-section normalizations of Table I and find no changes are required in the average parameters given above. These quantities may be compared with those from a global search between 10 and 50 MeV where the same set of parameters was found to be³:

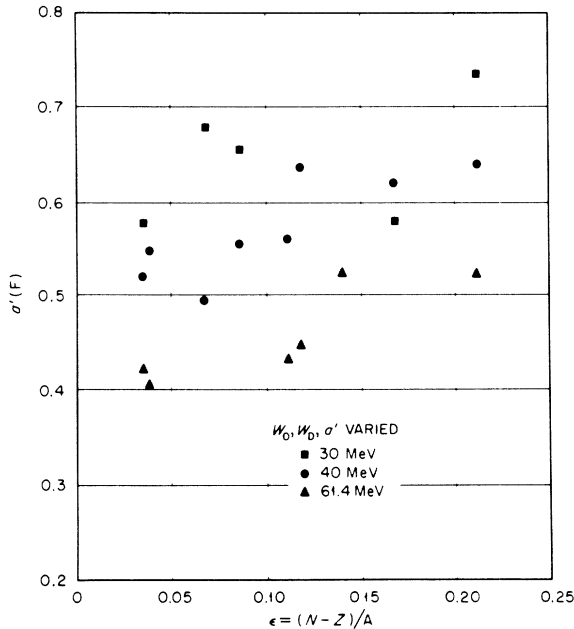


FIG. 14. Values of the imaginary diffusivity, a' , versus $\epsilon = (N - Z)/A$ from a three-parameter (W_0 , W_D , and a') optical-model fit to 30-, 40-, and 61.4-MeV proton elastic scattering, polarization, and total-reaction-cross-section data. The remaining optical-model parameters were taken from Ref. 1.

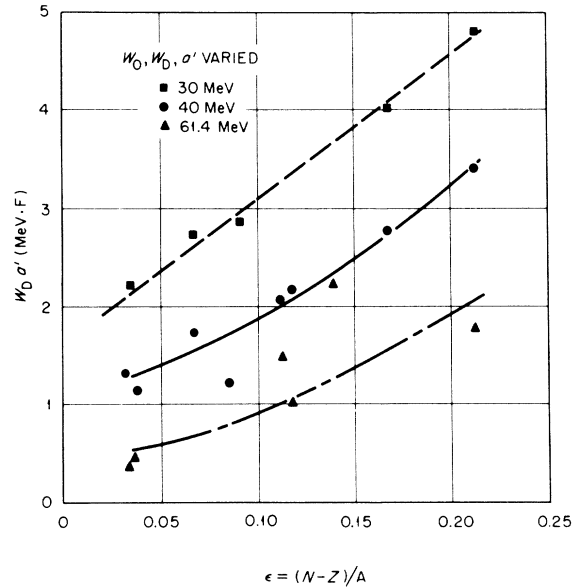


FIG. 15. The product of W_D and a' versus $\epsilon = (N - Z)/A$ from a three-parameter (W_0 , W_D , and a') optical-model fit to 30-, 40-, and 61.4-MeV proton elastic scattering, polarization, and total-reaction-cross-section data. The remaining optical-model parameters were taken from Ref. 1. The curves indicate the trends of the calculated values.

$$\begin{aligned}
 r_0 &= 1.17 \text{ F}, & V_s &= 6.2 \text{ MeV}, \\
 a &= 0.75 \text{ F}, & r_s &= 1.01 \text{ F}, \\
 r'_0 &= 1.32 \text{ F}, & a_s &= 0.75 \text{ F}, \\
 V_0 &= (54.0 - 0.32E_p + 0.4Z/A^{1/3} + 24.0\epsilon) \text{ MeV}.
 \end{aligned}
 \tag{4}$$

Using the Oak Ridge parameter set¹ [Eq. (3)] and the program GENOA,³⁹ we searched on W_0 , W_D , and a' to obtain a least-squares fit to elastic scattering, polarization, and reaction-cross-section data at 30, 40, and 60 MeV. At 30 MeV we used the elastic scattering data of Ridley and Turner³⁰ and the polarization data of Craig *et al.*⁴⁰ These two sets of data were obtained at energies differing by 1 MeV, but we have made no effort to correct for this. The 40-MeV elastic scattering and polarization data used were those of Fricke *et al.*¹ and the 61.4-MeV elastic scattering data were those of Fulmer *et al.*,¹⁴ and again we did not correct for the fact that the reaction-cross-section data were at a slightly lower energy. The errors on the reaction-cross-section data were arbitrarily reduced from the values tabulated in Sec. III until the reaction cross section contributed about 30% of the total χ^2 . In this way we were confident that the reaction-cross-section data would influence the χ^2 search.

The values of W_0 , W_D , and a' obtained by searching in the above manner are displayed graphically in Figs. 12–14 as functions of ϵ . At 40 MeV, where the largest body of systematic data is available, two trends are evident: (1) W_0 is 5.0 MeV and relatively constant for all targets, and (2) W_D

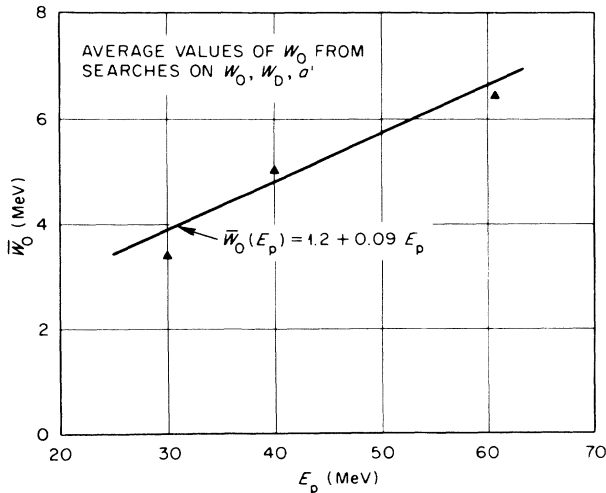


FIG. 16. Average volume absorption strengths, \bar{W}_0 , versus proton energy from a three-parameter (W_0 , W_D , and a') optical-model fit to 30-, 40-, and 61.4-MeV proton data. The average values are taken from Fig. 12 and the straight line is a representation of the energy dependence of \bar{W}_0 .

and a' tend to increase with increasing ϵ . It should be pointed out that such trends were not evident from the analysis of Fricke *et al.*¹ (see Table III of Ref. 1), who did not have reaction-cross-section data available. Similar trends are not as readily evident for the 30- and 61.4-MeV analyses except possibly for the lack of dependence of W_0 on ϵ . However, there is a definite decrease in the values of a' and W_D with increasing proton energy, while W_0 increases with increasing energy. We have parametrized the imaginary potential by including an energy dependence for W_0 and both an energy and ϵ dependence for W_D and a' .

Although the ϵ dependence of W_D and a' for the 30- and 60-MeV analysis is not well defined, the product $W_D a'$ shows a definite ϵ dependence as can be seen from Fig. 15. This behavior of the product $W_D a'$ becomes more pronounced if searches are made with a constant W_0 at each energy. Taking average values of W_0 at each energy from Fig. 12, we obtain the values plotted in Fig. 16. As is shown in Fig. 16 a reasonable parametrization is

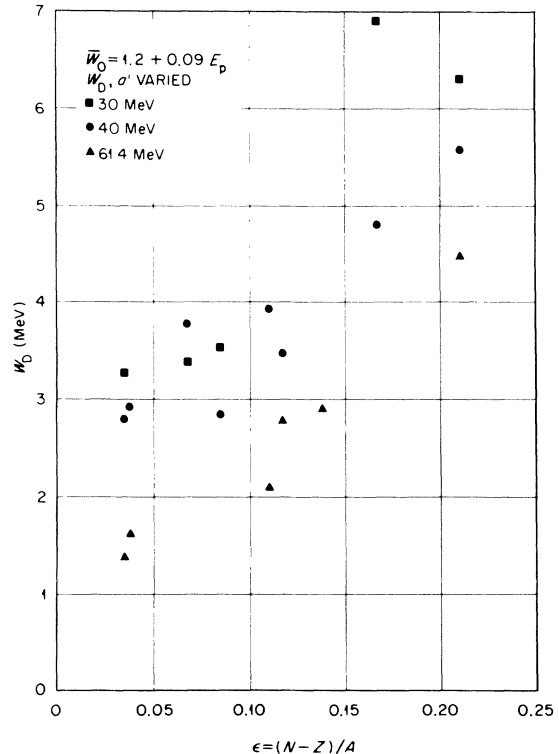


FIG. 17. Values of the surface absorption potential, W_D , versus $\epsilon = (N-Z)/A$ from a two-parameter (W_D and a') optical-model fit to 30-, 40-, and 61.4-MeV proton elastic scattering, polarization, and total-reaction-cross-section data. \bar{W}_0 values were calculated from $\bar{W}_0 = 1.2 + 0.09 E_p$ (Fig. 16) and the remaining optical-model parameters were taken from Ref. 1.

given by

$$W_0(E_p) = (1.2 + 0.09E_p) \text{ MeV}. \quad (5)$$

With this parametrization of W_0 , searches on W_D and a' gave the values shown in Figs. 17 and 18. An ϵ dependence, especially for W_D , is apparent from these results. Also evident from this analysis is an energy dependence for W_D which has been noted previously^{3,17} and an energy dependence for a' which has not appeared in previous analyses. A more striking ϵ dependence is displayed by the product $W_D a'$ shown in Fig. 19. Indeed, examination of these searches reveals that χ^2 is characterized by the value of the product $W_D a'$ and is relatively independent of individual values for W_D and a' . Since W_D shows a more regular ϵ behavior than a' (Fig. 17), we have tried to represent W_D by the form $W_D = \alpha + \beta E_p + \gamma \epsilon$ and then determine a similar form for a' so that the product $W_D a'$ approaches the trends of Fig. 19. Our resulting parametrization is

$$W_D = (4.2 - 0.05E_p + 15.5\epsilon) \text{ MeV}, \quad (6)$$

$$a' = (0.74 - 0.008E_p + 1.0\epsilon) \text{ F}. \quad (7)$$

This may be compared with the parameters found by Becchetti and Greenlees,³ who performed a

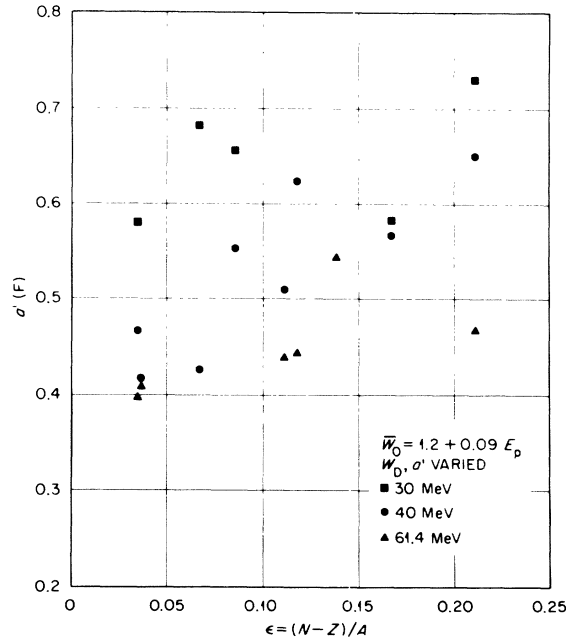


FIG. 18. Values of the imaginary diffusivity, a' , versus $\epsilon = (N-Z)/A$ from a two-parameter (W_D and a') optical-model fit to 30-, 40-, and 61.4-MeV proton elastic scattering, polarization, and total-reaction-cross-section data. \bar{W}_0 values were calculated from $\bar{W}_0 = 1.2 + 0.09 E_p$ (Fig. 16) and the remaining optical-model parameters were taken from Ref. 1.

global search on data between 10 and 50 MeV: $W_0 = (0.22E_p - 2.7) \text{ MeV}$, $W_D = (11.8 - 0.25E_p + 12.0\epsilon) \text{ MeV}$, $a' = (0.51 + 0.7\epsilon) \text{ F}$. The two models are compared in Table VI which gives calculated χ^2 values for elastic scattering and polarization and calculated reaction cross sections. On the basis of Table VI there is no way to choose between them. It is comforting that independent paths lead to very similar formulations.

A test of the adequacy of the above parametrization is afforded by the isotope dependence of the reaction cross sections shown in Figs. 9–11. The open symbols without error bars in Figs. 9–11 are the cross sections calculated with the parameters of Eqs. (4)–(7). As can be seen, the general dependence of the cross section with ϵ is quite well accounted for although the absolute values appear to be $\sim 10\%$ low at 60 MeV.

It is of interest to inquire if the asymmetry dependence of W_D and a' in Eqs. (6) and (7) are true isospin dependences in the sense that the ϵ term changes sign for a neutron beam. The isospin nature of the real potential, V_0 in Eq. (4), appears rather well established,³⁷ at least within the context of the conventional formulation used here.³⁵ Satchler,¹⁷ in an analysis of 30-MeV proton scattering, finds $W_D = 4.5 + 16\epsilon$ with a' fixed at 0.75 F. Applying his potential to 24-MeV neutron data, he finds a definite preference for $W_D = 4.5 - 16\epsilon$, which is

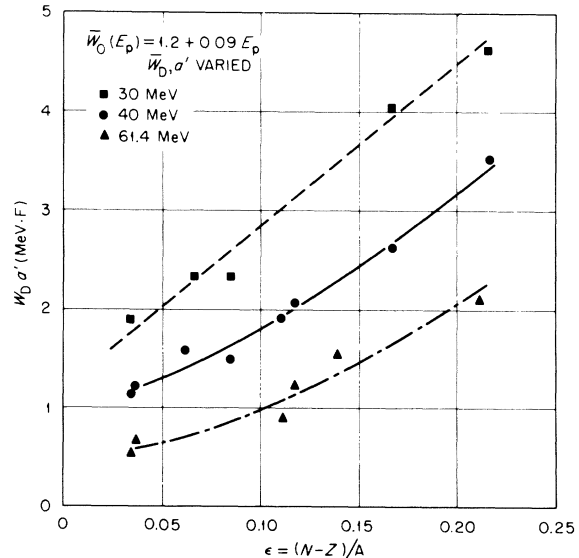


FIG. 19. The product of W_D and a' versus $\epsilon = (N-Z)/A$ from a two-parameter (W_D and a') optical-model fit to 30-, 40-, and 61.4-MeV proton elastic scattering, polarization, and total-reaction-cross-section data. \bar{W}_0 values were calculated from $\bar{W}_0 = 1.2 + 0.09 E_p$ (Fig. 16) and the remaining optical-model parameters were taken from Ref. 1. The curves indicate the trend of the calculated values.

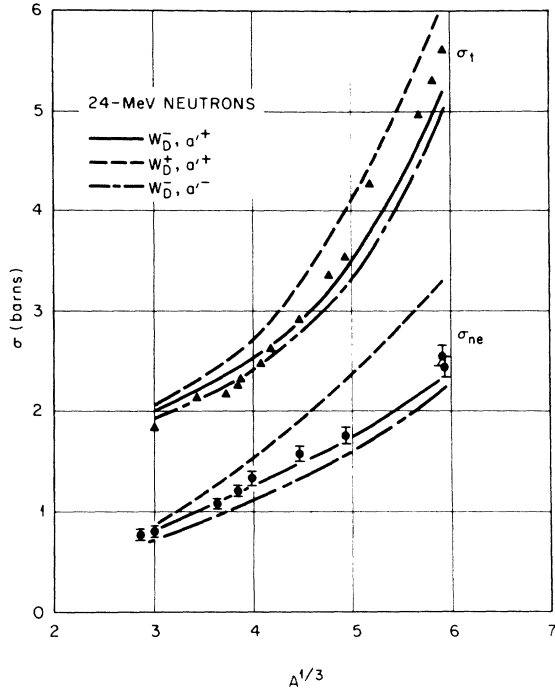


FIG. 20. Total reaction cross sections σ_t and nonelastic cross sections σ_{ne} for 24-MeV neutrons as a function of $A^{1/3}$. Total cross sections are from Ref. 41 and nonelastic cross sections are from Ref. 42. The calculated curves are for different assumptions concerning the sign of the asymmetry term in Eqs. (6') and (7').

consistent with a true isospin dependence. We have performed a similar comparison with our potential and the results are displayed in Fig. 20. The total-reaction-cross-section data in Fig. 20 are those of Peterson, Bratenahl, and Stoering⁴¹ and the nonelastic cross-section data from MacGregor, Ball, and Booth.⁴² The three calculated curves in Fig. 20 correspond to different combinations of the asymmetry dependence as defined by the following relations:

$$W_D^{\pm} = (4.2 - 0.05E \pm 15.5\epsilon) \text{ MeV} \quad (6')$$

$$a'^{\pm} = (0.74 - 0.008E \pm 1.0\epsilon) \text{ F.} \quad (7')$$

As noted by Satchler,¹⁷ the nonelastic neutron cross sections show a pronounced favoritism for W_D^- . We also detect in Fig. 20 a weak preference for a'^+ and thus the ϵ dependence of a' does not appear to be due to the difference in the $n-p$ and $p-p$ interaction, but, as argued by Satchler,³⁵ reflects a change in the geometry of the nuclear surface where most of the absorptions occur.

VI. SUMMARY

We report a total of 44 measurements of total reaction cross sections for 30.0-, 40.0-, 49.5-, and 60.8-MeV protons on separated isotope targets (Tables II-V). The 60.8-MeV measurements resolve a conflict between previous¹³ 60-MeV proton reaction cross sections on the one hand and 55-MeV neutron reaction cross sections¹⁵ and 60-MeV optical-model analysis of proton elastic scattering¹⁴ on the other hand. When plotted against $A^{2/3}$ (Fig. 7), the data fall on straight lines with the same slope at each energy. These data can be correlated with the expression $\sigma_R = \pi(\tau_0 A^{1/3} + \bar{\lambda})^2$, where $\bar{\lambda}$ is the de Broglie wave length of the proton beam and the radius parameter is well determined as $\tau_0 = 1.23 \pm 0.01$ F. Measurements on a series of Fe and Ni isotopes (Figs. 9 and 10) and on $N=28$ isotones (Fig. 11) verify¹¹ a dependence of the proton reaction cross section on the number of target neutrons.

The data are used to explore the $\epsilon = (N-Z)/A$ dependence of the imaginary optical potential. The real and spin-orbit parts of the optical potential and the imaginary radius are taken from an analysis¹ of elastic scattering and polarization data. We find a pronounced $(N-Z)/A$ dependence for the product $W_D a'$ (Figs. 15 and 19). The magnitude of the symmetry part of our imaginary surface potential [Eq. (6)] agrees with previous analyses.^{3,17} In addition to a symmetry dependence for the imaginary diffusivity, we also find evidence for an energy dependence in this parameter [Eq. (7)]. The imaginary optical-potential parametrization offered here, together with the previously determined Oak Ridge parameter set,¹ constitutes a zero-parameter optical model for protons in the energy range 30 to 60 MeV.

VII. ACKNOWLEDGMENTS

The authors wish to thank C. N. Waddell for some illuminating discussions at the start of this work. We are indebted to F. G. Perey for the use of his computer program GENOA and for his advice concerning the optical-model analysis. Data accumulation was greatly aided by the help of R. W. Rutkowski and W. J. Roberts and by the skillful operation of the cyclotron under the direction of A. W. Riikola. The flawless performance of the optical bench is due to the efforts of M. E. Wimberley and we are indebted to J. Z. Schnookboltz for the loan of some of the targets. One of us (J.J.H.M.) wishes to thank the Centre National de la Recherche Scientifique and NATO for their financial support, and the Oak Ridge National Laboratory for its generous hospitality.

*Research sponsored by the U. S. Atomic Energy Commission under contract with Union Carbide Corporation.

†Present address: Institut des Sciences Nucléaires, Grenoble, France.

‡Present address: Los Alamos Scientific Laboratory, Los Alamos, New Mexico.

§Present address: National Academy of Sciences, Washington, D. C.

¹M. P. Fricke, E. E. Gross, B. J. Morton, and A. Zucker, Phys. Rev. 156, 1207 (1967).

²G. R. Satchler, Nucl. Phys. A92, 273 (1967).

³F. D. Becchetti, Jr., and G. W. Greenlees, Phys. Rev. 182, 1190 (1969).

⁴T. J. Gooding, Nucl. Phys. 12, 241 (1959).

⁵B. D. Wilkins and G. Igo, Phys. Rev. 129, 2198 (1963).

⁶K. Bearpark, W. R. Graham, and G. Jones, Nucl. Phys. 73, 206 (1965).

⁷M. Q. Makino, C. N. Waddell, and R. M. Eisberg, Nucl. Phys. 50, 145 (1964).

⁸M. Q. Makino, C. N. Waddell, R. M. Eisberg, and J. Hestenes, Phys. Letters 9, 178 (1964).

⁹R. E. Pollock and G. Schrank, Phys. Rev. 140, B575 (1965).

¹⁰M. Q. Makino, C. N. Waddell, and R. M. Eisberg, Nucl. Phys. 68, 378 (1965).

¹¹J. F. Dicello, G. J. Igo, and M. L. Roush, Phys. Rev. 157, 1001 (1967).

¹²J. F. Dicello and G. Igo, Phys. Rev. C 2, 488 (1970).

¹³V. Meyer, R. M. Eisberg, and R. F. Carlson, Phys. Rev. 117, 1334 (1960).

¹⁴C. B. Fulmer, J. B. Ball, A. Scott, and M. L. Whiten, Phys. Rev. 181, 1565 (1969).

¹⁵R. G. P. Voss and R. Wilson, Proc. Roy. Soc. (London) A236, 41 (1956).

¹⁶F. G. Perey, in *Proceedings of the Second International Symposium on Polarization Phenomena of Nucleons, Karlsruhe, 1965*, edited by P. Huber and H. Schopper (Birkhäuser Verlag, Basel, Switzerland, 1966), p. 191.

¹⁷G. R. Satchler, Nucl. Phys. A91, 75 (1967).

¹⁸J. J. H. Menet, E. E. Gross, J. J. Malanify, and A. Zucker, Phys. Rev. Letters 22, 1128 (1969).

¹⁹D. F. Measday, Nucl. Instr. Methods 34, 353 (1965).

²⁰F. E. Bertrand and R. W. Peelle, to be published.

²¹M. P. Fricke, E. E. Gross, and A. Zucker, Phys. Rev. 163, 1153 (1967).

²²R. A. Ricci, J. C. Jacmart, M. Liu, M. Riou, and C. Ruhla, Nucl. Phys. A91, 609 (1967).

²³S. F. Eccles, H. F. Lutz, and V. A. Madsen, Phys. Rev. 141, 1067 (1965).

²⁴A. L. McCarthy and G. M. Crawley, Phys. Rev. 150, 935 (1966).

²⁵O. N. Jarvis, B. G. Harvey, D. L. Hendrie, and J. Mahoney, Nucl. Phys. A102, 625 (1967).

²⁶B. W. Ridley, J. F. Turner, and J. C. Kerr, P. L. A. Progress Report No. NIRL/R/81, 40, 1964 (unpublished).

²⁷G. M. Crawley and G. T. Garvey, Phys. Rev. 167, 1070 (1968).

²⁸W. S. Gray, R. A. Kenefick, J. J. Kraushaar, and G. R. Satchler, Phys. Rev. 142, 735 (1966).

²⁹H. O. Funsten, N. R. Roberson, and E. Rost, Phys. Rev. 134, B117 (1964).

³⁰B. W. Ridley and J. F. Turner, Nucl. Phys. 58, 497 (1964).

³¹C. N. Waddell, private communication. This value represents a corrected value from that reported in Ref. 7.

³²J. M. Cameron, R. F. Carlson, W. F. McGill, and J. R. Richardson, University of California at Los Angeles Cyclotron Laboratory Report, July 1968 (unpublished).

³³J. F. Turner, B. W. Ridley, P. E. Cavanagh, C. A. Gard, and A. G. Hardacre, Nucl. Phys. 58, 509 (1964).

³⁴R. A. Giles and E. J. Burge, Nucl. Phys. 50, 327 (1964).

³⁵G. R. Satchler, in *Isospin in Nuclear Physics*, edited by D. H. Wilkinson (North-Holland Publishing Company, Amsterdam, The Netherlands, 1969), p. 389.

³⁶J. Hüfner and H. A. Weidenmüller, Comments Nucl. Particle Phys. 4, 121 (1970), and references therein.

³⁷F. G. Perey, Phys. Rev. 131, 745 (1963).

³⁸G. R. Satchler, Nucl. Phys. A100, 481 (1967).

³⁹F. G. Perey, private communication.

⁴⁰R. M. Craig, J. C. Dore, G. W. Greenlees, J. S. Lilley, and J. Lowe, Nucl. Phys. 58, 515 (1964).

⁴¹J. M. Peterson, A. Bratenahl, and J. P. Stoering, Phys. Rev. 120, 521 (1960).

⁴²M. H. MacGregor, M. P. Ball, and R. Booth, Phys. Rev. 111, 1155 (1958).

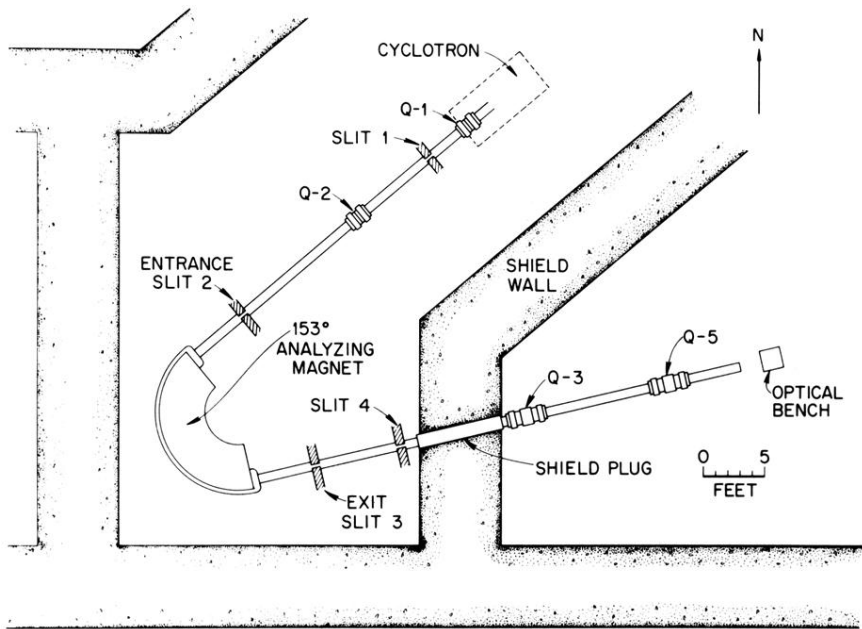


FIG. 5. Schematic layout of the beam optics.